Optimal Design of a Trickle Bed Reactor for Light Fuel Oxidative Desulfurization based on Experiments and Modelling

Amer T. Nawaf [1], Saba A. Gheni [1], Aysar T. Jarullah [1,2],

Iqbal M. Mujtaba[3,4]

[1]Chemical Engineering Department, College of Engineering, Tikrit University, IRAQ

[2] Email: A.T.Jarullah@tu.edu.iq

[3] Chemical & Process Engineering Division, School of Engineering, University of Bradford,

Bradford BD7 1DP, UK

[4] Email: I.M.Mujtaba@bradford.ac.uk

Abstract

In this work, the performance of oxidative desulfurization (ODS) of dibenzothiophene (DBT) in light gas oil (LGO) is evaluated with a homemade manganese oxide (MnO_2/γ-Al_2O_3) catalyst. The catalyst is prepared by Incipient Wetness Impregnation (**IWI**) method with air under moderate operating conditions. The effect of different reaction parameters such as reaction temperature, liquid hour space velocity and initial concentration of DBT are also investigated experimentally.

Developing a detailed and a validated trickle bed reactor (TBR) process model that can be employed for design and optimization of the ODS process, it is important to develop kinetic models for the relevant reactions with high accuracy. Best kinetic model for the ODS process taking into account hydrodynamic factors (mainly, catalyst effectiveness factor, catalyst wetting efficiency and internal diffusion) and the physical properties affecting the oxidation process is developed utilizing data from pilot plant experiments. An optimization technique based upon the minimization of the sum of the squared error between the experimental and predicted composition of oxidation process is used to determine the best parameters of the kinetic models. The predicted product conversion showed very good agreement with the experimental data for a wide range of the operating condition with absolute average errors less than 5%.

Key words

Oxidative desulfurization, Dibenzothiophene, Trickle bed reactor, Mathematical model, Kinetic parameters estimation.

1. Introduction

Feedstock (fuels) containing different sulphur compounds, thiols, sulfides, disulfiedes and thiophenes cause severe environmental pollution by generating SO_x and airborne particulate emissions through combustion catalyst poisoning of downstream process and corrosion equipment of the refinery (mainly pipe, pump, heat exchanger and reactor). The sulphur level in diesel fuel according to US guideline should be less than 15 ppm[1]. Therefore, desulfurization of liquid fuel is very essential in the petroleum processing industry.

The conventional sulphur removing method in petroleum refining industry is called a catalytic hydrodesulfurization (HDS) process. The purpose of HDS is to convert the sulphur compounds into hydrogen sulfied and hydrocarbons, but such process renders difficulty in removing sulphur compounds (namely benzothiophene (BT) and dibenzothiophene (DBT)) due to high resistant of BT and DBT to hydrogenation process and require use of more severe operating conditions (temperature and pressure) including more active catalysts and high volume of hydrogen making this operation more expensive in comparison to other operations[2].

Recently, oxidative desulfurization process (ODS) of feedstock (fuels) has attracted a great deal of attention among researchers due to its advantages, such as high efficiency and mild reaction conditions in terms of temperature and liquid hourly space velocity (LHSV) and almost constant pressure (atmospheric pressure) making such process much safer[3-11].

The oxidants for oxidative desulfurization includes hydrogen peroxide (H_2O_2), peracids, oxygen[12-14]. The catalyst for oxidative desulfurization are amphiphilic quaternary ammonium phosphomolybdate[15], polyoxometalates[11], methyltrioxorhenium[11] or various supported catalysts, i.e. MoO_3, CrO_3 and WO_3 supported on alumina[15-17], manganese oxide on alumina[18] and CuO-ZnO on alumina[19] (commercial catalysts).

In ODS process, the organic sulphur compounds (mercaptans, sulphides, and thiophenes) are converted directly into the corresponding oxidized sulphur compounds, disulfides, sulphones, and sulfoxides that remain in the product and the total sulphur content of the treated stock is not reduced. But the chemical and physical properties of oxidized organic sulphur compounds are significantly different from those of hydrocarbon in fuel oil (more polar)[20-22]. Therefore, they can be easily removed by separation process such as solvent extraction[23,24] and adsorption[25-27].

In petroleum refining, petrochemical and chemical processes, TBR is employed extensively for gas-liquid-solid catalyzed systems. Down flow gas and liquid in TBR over a porous catalyst particle is extremely complex and the liquids may or may not completely wet the catalyst surface. Understanding the behavior of TBR taking into considerations the hydrodynamic parameters (mainly pressure drop, liquid holdup and wetting efficiency) that should be accounted for in any modelling effort together with the description of reaction kinetics and transport in catalyst

particles, plays a significant role in designing of such reactor. Changing in the wettability refers to the change in liquid flow leading to increase or decrease in the fractional coverage of catalyst particle, i.e. wetting efficiency[28].

The present study is aimed to obtain an optimal design of TBR by developing kinetic model based upon the pilot plant experiments with a homemade catalyst for the oxidative desulfurization of DBT in light gas oil under moderate operating conditions using air as oxidant. The optimization technique is utilized to obtain the best kinetic parameters of the TBR processes for the reactions considered in this work. The gPROMS (**g**eneral **PRO**cess **M**odelling **S**ystem) software has been employed for modelling, simulation and optimization operations. The optimization problem is posed as a Non-Linear Programming (NLP) problem and is solved using a Successive Quadratic Programming (SQP) method within the gPROMS package.

2. Experimental Work

2.1 Materials

A γ-Al_2O_3 with a surface area of 289 m^2/g, pore volume of 0.5367 cm^3/g, bulk density 0.671 g/cm^3 and particle diameter of 1.6 mm (spherical) was purchased from Aldrich. Dibenzothiophene (DBT) is the model sulphur compound selected to evaluate the reactivity of sulphur in an oxidation reaction (DBT has also been purchased from Aldrich with purity >98%). Light gas oil (LGO) was obtained from ***North Refineries Company*** **in Iraq**. The physical properties of feedstock (LGO) is illustrated in Table 1. Air was used as oxidant in oxidative desulfurization.

2.2 Catalyst Preparation

The (MnO_2/γ-Al_2O_3) catalysts with a 13%MnO_2 were prepared by **IWI** method. 100 gm of γ-Al_2O_3 is dried in the oven at 293K for 4 hours. This step is necessary to remove any moisture in the support before impregnation. Then, 15 gm of manganese acetate (the properties of the active compounds is shown in Table 2) is added to 50 ml of deionized water (was obtained from ***Samarra Company***) and the solution is stirred for 1hour at room temperature utilizing a magnetic stirrer. γ-Al_2O_3 is first put in the flask under vacuum condition (using vacuum pump) to remove gases out of support pores, then the solution prepared is added to γ-Al_2O_3 at the rate of 15 to 20 (drop per minute) with continuous stirring until all the solution is impregnated under constant temperature of 373 K employing a bath water (a simplified diagram of the catalyst preparation apparatus is shown in Figure 1). The impregnated γ-Al_2O_3 is dried overnight in the oven at 393K to eliminate any remaining water found upon the γ-Al_2O_3. After that, the dried catalyst is calcinated for 5 hours in the oven at 823K under laminar air flow. This step is necessary as most of the metal salts loaded upon the γ-Al_2O_3 will be converted into their corresponding metal oxides leading to deposition of active metal oxide over catalyst support and acquisition of desired physical and chemical properties of the catalyst. Figure 2 shows the flow chart of the preparation steps. Calcination process is carried out in ***Fertilizer Northern Company- Baiji***.

2.3 Oxidation Operation in Trickle Bed Reactor

2.3.1 Apparatus and procedure

The continuous oxidation of LGO has been conducted in a packed bed reactor operating a co-currently (down-flow). The TBR consists of a SS-310 tubular reactor, 77 cm in length with an inner diameter of 1.6 cm and is controlled automatically by 4 sections of 15 cm height steel-jacket heaters. The pilot plant experiments have been conducted in **Chemical Engineering Department/ College of Engineering/ Tikrit University.**

The liquid feedstock is charged into a feed tank, which is connected to a high-pressure metering pump (dosing pump) that can dispense flow rates from 0.0 to 1.65 Liter/ h at constant pressure of 20 bar. The oxidant is fed (air gas) by a high pressure air compressor equipped with a pressure controller to keep the process under constant operating pressure. Gas flow-meter coupled with a high precision valve is used to measure and control the flow rate of the gas. The liquid and gas streams are mixed and then introduced into the reactor at the required temperature. The mixture flows along the packed bed of the catalyst enclosed between two layers of inert material. The length of the reactor is divided into three part. The first part, of length (30 to 35% vol.) was packed with inert particles. The second section of length (40% vol.) was packed with manganese oxide catalyst. The bottom section contained also a packing of inert particles of length (30 to 35% vol.) in order to serve as disengaging section[29]. The outlet solution goes to a liquid-gas separation, regularly, where liquid samples are collected for analysis. Figure 3 illustrates the experimental setup and the description specifications of the system is shown in Table 3.

2.3.2 Experimental Runs

The following steps are performed to prepare and run the experiments:

1. Check the system leaks by pressurizing nitrogen gas to 5 bar for 24 hours then depressurize nitrogen to ensure the normal runs at 2 bar.
2. Ensure that the cooling water is flowing through the heat exchanger. The temperature of the cooling jackets should not exceed 293K to prevent vaporization of light components present in LGO.
3. Flow the nitrogen gas into the system in order to check any leaks and get rid of any remaining gases and liquid of previous run.
4. Prepare model oil by dissolving DBT in LGO with corresponding S-content of 500, 800, 1000ppm, respectively.
5. Flow the air gas through the reactor at pressure of 2 bar.
6. Set the temperature controller to the feed injection temperature (should be lower than the steady state operation temperature). Note that the feed injection temperature is not constant and depends on steady state temperature, where the applied temperature is ranged between 403 and 473K.

7. Turn on the dosing pump at a certain LGO flow rates (LHSV from 1 to $3h^{-1}$). The discharge valve is opened when the air gas temperature reaches to the feed injection temperature.

8. Increase the temperature until steady state temperature is obtained, then the sample is collected.

9. Switch off LGO dosing pump with air gas kept flowing to back wash of any remaining LGO. The air valve is then closed and nitrogen gas is flown inside the system for removing air gas.

2.4 The Sulphur Content in Model Oil (GC-capillary Chromatography)

DBT content in feedstock and product are calculated computationally via Gc-capillary chromatography, having the following specifications:

- Colum : CP-Sil 8 CB fused silica WCOT
  30 m x 0.25 mm , df = 0.25 µm
  Cat. No. CP8751
- Temperature : 40 ^{o}C (2 min) → 280 ^{o}C, 10 ^{o}C/min
- Carrier gas : He, 39 cm/s, 128 KPa (1.28 bar, 18.6 psi)
- Injector : Splitless,
  : T = 250 ^{o}C
- Detector : FID,
  T = 300 ^{o}C
- Sample size : 2 µm
- Concentration range : 10 ppm

The estimation of the outlet concentration of DBT unreacted can be achieved by reading the value from the computer.

3. Description of the Reactor Models

When developing a generalized reactor model, nothing should be neglected a priori, but all the resistances and others terms must be included in mass and heat balance equations[30]. However, such a model can be very complex and difficult to solve, even supposing that all the parameters involved are available, and thus some assumptions are still needed. The assumptions, of course, have to be well supported and preferably validated with experimental data. The mass and heat balance equations in the case of the generalized reactor model for processing are detailed, which have been developed with the following assumptions: liquid and gas properties (superficial velocities, mass and heat dispersion coefficients, specific heats, holdups, and densities), catalyst properties (porosity, size, activity, effectiveness, etc.), wetting efficiency, and bed void fraction are constant along the entire catalyst bed.

Here, the following assumptions are used to create the mathematical models for ODS processes of DBT present in LGO using TBR:

- The experimental unit is in steady state operation.
- Isothermal and constant pressure operation of the reactor.
- Negligible back mixing effects (high value of Peclet number).
- The liquid is saturated with gas at all times and gaseous reactant is present in large excess.
- No evaporation or condensation occurs from or into the liquid phase.

The required data and available tools with the assumptions for modelling and simulation processes light gas oil desulfurization are tabulated in Figure 4.

3.1 Models Based on Kinetics

Several investigators have indicated that pore diffusion impacts can be taken into considerations within the framework of an effective or apparent reaction rate constant (in other words, multiplying intrinsic reaction rate constant by effectiveness factor), in the purpose of formulating a pseudo homogeneous basic plug flow model which is adequate for describing the progress of chemical reactions in the liquid phase of a TBR. Mass balance equations in the TBR for oxidative desulfurization operation can be described with the following set of differential and algebraic equations. The general mass balance over catalytic reactor for DBT compound entering the reactor is:

[Input] = [Output] + [generation by reaction] + [Accumulation] (1)

Since $F_{DBT} = C_{DBT}\, v_L$

$$F_{DBT} = (F_{DBT} + dF_{DBT}) + (-r_{DBT})dV \quad (2)$$

After separation of variables and inclusion of space-velocity concept (LHSV= v_L /V), the equation that accounts for DBT compound in the differential section of the catalyst is written as:

$$\tau = C_{DBT0} \int_0^{X_{DBTf}} \frac{dX_{DBT}}{-r_{DBT}} \quad (3)$$

Where,$(-r_{DBT})$ is certainly dependent on the concentration or conversion of materials.

The chemical complexity of the reaction may be reasonably taken into consideration by assuming *n*th order kinetics ($-r_{DBT} = K_{app} C_{DBT}^{n}$).

Apparent kinetics can be related with the intrinsic kinetics considering internal diffusion and TBR hydrodynamic effects as follows[31]:

$$K_{app} = \eta_0 \eta_{ce} K_{in} \quad (4)$$

Where η_0 , η_{ce} catalyst effectiveness factor and catalyst wetting efficiency respectively.

The chemical reaction rate equation is stated as:

$$-r_{DBT} = -\frac{dc_{DBT}}{dt} = K_{in}\eta_0\eta_{ce}C_{DBT}^{n} \tag{5}$$

Reaction rate with respect to Arrhenius equation applied in this equation is:

$$-r_{DBT} = -\frac{dc_{DBT}}{dt} = K_0 e^{-\frac{EA}{RT}}\eta_0\ \eta_{ce}C_{DBT}^{n} \tag{6}$$

After integration:

$$\frac{1}{n-1}\left[\frac{1}{C_{DBTf}^{n-1}} - \frac{1}{C_{DBT0}^{n-1}}\right] = \frac{k_{app}}{LHSV} \tag{7}$$

Also

$$\frac{1}{n-1}\left[\frac{1}{C_{DBTf}^{n-1}} - \frac{1}{C_{DBT0}^{n-1}}\right] = \frac{\eta_0\eta_{ce}K_{in}}{LHSV} \tag{8}$$

Dudukovic[32] suggested that catalyst effectiveness factor and partial surface-wetting effects being coupled local phenomena in TBRs are a function of the Thiele modulus for nonvolatile liquid reactants in liquid-phase reactant-limited reactions, considering both incomplete external wetting and fractional pore fill-up (or internal partial wetting). Fractional pore fill-up will depend on the catalyst pore structure and physical properties (particularly on surface tensions) of the gas-liquid-solid system involved. The effectiveness factor of independent reactions can be defined as the ratio of the volumetric average of the reaction rate into the particle to the reaction rate at the surface of the particle as proposed by[33]:

$$\eta_0 = \frac{3(\Phi\coth\Phi - 1)}{\Phi^2} \tag{9}$$

The generalized Thiele modulus (Φ) for n[th]-order irreversible reaction is[34]:

$$\Phi = \frac{V_P}{S_P}\sqrt{\left(\left(\frac{n+1}{2}\right)\frac{K_{in}(C_{DBT})^{n-1}\left(\frac{\rho_B}{1-\epsilon_B}\right)}{D_{ei}}\right)} \tag{10}$$

The effective diffusivity (D_{ei}), by means of which the structure (porosity and tortuosity) of the pore network inside the particle is taken into account within the modelling[21].

$$D_{ei} = \frac{\rho_p V_g}{\mathcal{T}}\frac{1}{\frac{1}{D_{mi}} + \frac{1}{D_{ki}}} \tag{11}$$

Where $(\rho_p * V_g)$ equals to the catalyst porosity, V_g IS total pore volume.

The effective diffusivity inside the catalyst particle includes two diffusion contributions: Knudsen diffusivity D_{ki} and molecular diffusivity D_{mi}. Knudsen diffusivity factor (D_{ki}) is estimated as follows[35]:

$$D_{ki} = 9700\left(\frac{2V_g}{S_g}\right)\left(\frac{T}{MW_i}\right)^{0.5} \tag{12}$$

Where $(\frac{2V_g}{S_g})$ equal to r_g (mean pore radius)[27].

The molecular diffusivity (D_{mi}) is evaluated by **Tyn-Calus** equation [36,37]:

$$D_{mi} = 8.93 \times 10^{-8} \frac{v_L^{0.267} T}{v_{DBT}^{0.433} \mu_L} \quad (13)$$

The molar volume (v_{DBT}) of LGO, and the critical specific volume (v_{cL}) of LGO is estimated by a **Riazi–Daubert** correlation[38]:

$$V_L = 0.285(v_{cL})^{1.048} \quad (14)$$

$$v_{cL} = (7.5214 \times 10^{-3}(T_{meABP})^{0.2896}(\rho_{15.6})^{-0.7666})MW_L \quad (15)$$

The tortuosity factor $(\mathcal{T})$ of the pore network is used in the calculation of D_{ei} because the pores are not oriented along the normal direction from the surface to the center of the catalyst particle[35], which is:

$$\frac{1}{\mathcal{T}} = \frac{\epsilon_S}{1-\frac{1}{2}\log(\epsilon_S)} \quad (16)$$

Experiments in bench-scale TBRs have shown that distribution of liquid over catalyst particle bed can be extremely non-uniform at the low-liquid space velocities prevailing in bench-scale reactors compared with commercial scale reactors. This liquid maldistribution within the catalyst bed causes an ineffective use of catalyst active sites also known as ‘‘incomplete catalyst wetting’’. This impact can be reduced considerably by improving the uniformity of liquid distribution with increasing superficial liquid velocity and reducing catalyst particles size. In catalyst-wetting based models, the catalyst utilization is assumed to be proportional to the fraction of the outside catalyst surface effectively wetted by the flowing liquid also known as ‘‘effective catalyst wetting,’’ which is defined as the ratio of external wetted area to total area of catalyst particle.

The external catalyst surface η_{ce}, can be determined at atmospheric pressure employing the correlation of **Al-Dahhan and Dudukovic**[39].

$$\eta_{ce} = 1.617 Re_L^{0.146} Ga_L^{-0.071} \quad (17)$$

Modified Reynolds number is stated as:

$$Re_L^{''} = \frac{\rho_L u_L d_p}{\mu_L(1-\epsilon_B)} \quad (18)$$

Modified Galileo number:

$$Ga_L^{''} = \frac{d_p^3 \rho_L^2 g \epsilon_B^3}{\mu_L^2(1-\epsilon_B)^3} \quad (19)$$

Bed void fraction (or bed porosity, ϵ_B) for undiluted catalyst bed can be estimated with the following correlation reported by **Froment and Bischoff**[40], and presented by **Jarullah et al.**[41].

$$\epsilon_B = 0.38 + 0.073 \left(1 + \frac{\left(\frac{d_t}{d_{pe}} - 2\right)^2}{\left(\frac{d_t}{d_{pe}}\right)^2} \right) \quad (20)$$

The external volume (V_P) and surface of catalyst (S_P) of regular shape (sphere) are calculated using:.

$$V_P = \frac{4}{3}\pi\left(r_p\right)^3 \quad (21)$$

$$S_P = 4\pi\left(r_p\right)^2 \quad (22)$$

The density of LGO (ρ_L) as a function of temperature and pressure is calculated by the **Standing-Katz** equation[42]:

$$\rho_L = \rho_o + \Delta\rho_p - \Delta\rho_T \quad (23)$$

The pressure depends on liquid density and is represented by the following equation:

$$\Delta\rho_p = (0.167 + 16.181 \times 10^{-0.0425\rho_0}).\ \left(\frac{P}{1000}\right) - 0.01 \times (0.299 + 263 \times 10^{-0.0603\rho_0}).\left(\frac{P}{1000}\right)^2 \quad (24)$$

The temperature used for correction of the liquid density in this equation:

$$\Delta\rho_T = (0.0133 + 152.4(\rho_o + \Delta\rho_P)^{-2.45}).(T - 520)\ -\left(8.1 \times 10^{-6} - 0.0622 \times 10^{-0.764(\rho_0 + \Delta\rho_P)}\right).\ (T - 520)^2 \quad (25)$$

Glaso's equation has been used as a generalized mathematical equation for oil viscosity. The equation has the following form[43]:

$$\mu_L = 3.141 \times 10^{10}(T - 460)^{-3.444}[\log_{10} API]^a \quad (26)$$

$$a = 10.313[\log_{10}(T - 460)] - 36.447 \quad (27)$$

The (API) can be calculated using:

$$API = \frac{141.5}{Sp.gr_{15.6}} - 131.5 \quad (28)$$

The TBR process model (Equations 1 to 28) is developed and solved within the gPROMS (**g**eneral **PRO**cess **Modelling** **S**ystem) package.

4. Estimation of Model Parameters

For solving the set of ordinary differential equations (ODEs) (for the steady-state regime) or the set of PDEs (for the dynamic regime), it is important to estimate a lot of parameters and chemical properties of the system. Those parameters can be evaluated with existing correlations, whose accuracy is of great importance for the entire state of robustness of the reactor model.

Some parameters that account for bed characterization are experimentally measurable, others are experimental or can be obtained through simulations, and others are empirical. Of course, although it is better to obtain the local porosity experimentally, the measurements require the use of advanced techniques and can be expensive. Therefore, often computational calculations are preferred.

The experimental data of oxidation reaction is adjusted with a simple power law kinetic model. Plug-flow behavior is considered, and the reaction system was modeled by eq. 5:

$$-r_{DBT} = -\frac{dc_{DBT}}{dt} = K_{in}\eta_0\eta_{ce}C_{DBT}^{n}$$

Estimated yields are evaluated by integration of equation 5, where $\mathbf{C_{DBT0}}$ is the feed concentration of DBT:

$$C_{DBTf}^{calc.} = \left(\frac{C_{DBT0}^{n-1}\times LHSV}{C_{DBT0}^{n-1}\eta_0\times\eta_{ce}\times K_{in}\times(n-1)+LHSV}\right)^{1/(n-1)} \quad (29)$$

C_{DBTf} is the product concentration of DBT, **LHSV** is the liquid hourly space velocity and n is the reaction order.

For parameter calculation, the objective function, ***SSE***, as given below, is minimized:

$$SSE = \sum_{n=1}^{N_t}\left(C_{DBT}^{meas.} - C_{DBT}^{prid.}\right)^2 \quad (30)$$

In the above equation, N_t , $C_{DBT}^{meas.}$ **and** $C_{DBT}^{prid.}$ are the numbers of test runs, the measured product yield and the predicted one by model, respectively. The calculation step starts with suggested kinetic parameters reported in the literature, to evaluate the composition of all fractions using the process model developed in gPROMS (general Process Modelling System). The kinetic parameters are then updated by minimizing SSE in the optimization problem presented below. Although, there are others methods and software for parameter estimation available in the literature[44], we have used the method available within gPROMS software as it provides state-of-the art parameter estimation capabilities which includes extensive statistical analysis using the information contained in nonlinear process models.

4.1 Optimization Problem Formulation for Parameter Estimation

The parameter estimation problem formulation can be stated as follows:

Given	The reactor configuration, the catalyst, the feedstock, the process conditions
Optimize	The reaction orders of oxidation reaction (n_1), reaction rate constants (k) at different temperatures (403K, 443K, 473K, respectively for two catalysts).
So as to minimize	The sum of square errors (*SSE*).
Subject to	Constraints on the conversion and linear bounds on all optimization variables.

Mathematically, the problem can be presented as:

Min.	***SSE***
$n^j, k_i^j,$	***(i=1-3, j= MnO_2/γ-Al_2O_3)***
S.t.	$\mathbf{f(z, x(z), u(z), v) = 0}$
	$C_L \leq C \leq C_U$
	$n^j{}_L \leq n^j \leq n^j{}_U$
	$k_i^j{}_L \leq k_i^j \leq k_i^j{}_U$

f(z**, x(**z**), u(**z**), v) = 0** represents the process models presented previously, where z is the independent variable, **u(**z**)** is the decision variable, **x(**z**)** gives the set of all differential and algebraic variables, and **v** represents the design variables. **C** is the concentration, and $\boldsymbol{C_L}$ and $\boldsymbol{C_U}$ are the lower and upper bounds of concentration. **L** and **U** are the lower and upper bound.

The optimization solution method used by gPROMS is a two-step method known as feasible path approach. The first step performs the simulation to converge all the equality constraints (described by $\boldsymbol{f}$) and to satisfy the inequality constraints. The second step performs the optimization (updates the values of the decision variables such as the kinetic parameters). The optimization problem is posed as a Non-Linear Programming (NLP) problem and is solved using a Successive Quadratic Programming (SQP) method within gPROMS software. The values of constant parameters used in these models are given in Table 4. Note, equal weightings have been used for all parameters being estimated in this optimisation. Also note, as we used only one reaction rate equation (Equation 5) based on simple power law kinetic model, reformulation of the kinetic model (as suggested by Buzzi-Ferraris and Manenti[45] for complex kinetic model with multiple reactions) was not necessary.

5. Results and Discussions

5.1 Experimental Section

Oxidative desulfurization of the DBT in LGO as model fuel was performed in the catalytic oxidation using air as oxidant. In this process, from the temperature was varied from 403 to 473K, liquid hourly space velocity was varied from 1 to $3h^{-1}$ and the initial concentration of DBT was varied from 500 to 1000ppm using manganese oxide catalyst.

5.1.1 Influence of the Catalyst

DBT is oxidized to the sulphone by (MnO_2/γ-Al_2O_3) using air as oxidant. The conversion of DBT increased with increasing temperature as shown in the Figure 5a. The influences of (MnO_2/γ-Al_2O_3) upon dibenzothiophene and reaction conditions are presented in Table 5.

The effect of metal oxide loading and reaction temperature below 403K, results in no oxidation reaction. However, in the case of metal oxide loading catalyst, higher metal loading led to higher conversion at temperature 403, 443, 473K and liquid hourly space velocity 1, 2, $3h^{-1}$. The optimal results were obtained with catalyst (13% MnO_2/γ-Al_2O_3), 473K and $1h^{-1}$.

5.1.2 The Influence of Reaction Temperature

Reaction temperature has a significant effect on DBT conversion. The catalytic activity of (MnO_2/γ-Al_2O_3) is high even at mild temperature of 443K, where the efficiency of the chemical reaction is 50.9% for LHSV of $1h^{-1}$. With an increase

in oxidation reaction temperature, the efficiency increases significantly, and DBT conversion reaches 78.1% at 473K and 800ppm as presented in Figure 5b.

5.1.3 The Influence of Liquid Hourly Space Velocity on Oxidation Process

The increase in LHSV usually accompanies with shortening in the contact time between reactants and catalyst particles. Higher liquid flow rates gives greater liquid holdup, which evidently decreases the contact of liquid and gas reactants at the catalyst active site by increasing film thickness. Thus, more oxidation reaction can be occurred. Figure 5c shows the impact of LHSV on the process.

5.1.4 Influence of Initial DBT Concentration

The influence of initial concentration of DBT is studied at 500, 800, and 1000 ppm. Figure 5d (also Table 5) showed that the conversion has been affected by the initial concentration of DBT. It is obvious that an increase of initial concentration will raise the rate of conversion. This behavior can be attributed to the fact that increasing initial organic sulphur compounds can give more chances for the reaction to be occurred, also there is no irreversible adsorption between active site (which is responsible for oxidation reaction) and oxidized DBT to sulphone and sulphoxide.

5.2 Estimation of Kinetic Parameters

The kinetic parameters for light gas oil oxidation process presented in this work have been estimated utilizing the experimental data from trickle bed reactor. Using the kinetic parameters reported in the literature as an initial estimate, the composition of all concentrations has been calculated by application of model equations in gPROMS. The comparison between experimental data and predicted data are illustrated in Table 6. As can be seen from these Tables, there are a large variation between predicted and experimental values. Hence, optimization technique has been employed on model parameters for minimizing this variation. The optimal kinetic parameters obtained via optimization technique for ODS process can be summarized as follow:

Parameter	**Value**	**Units**
n	1.300	(-)
K1@T_1	0.406	$(h^{-1} * (Wt)^{-0.30077})$
K2@T_2	0.738	$(h^{-1} * (Wt)^{-0.30077})$
K3@T_3	1.922	$(h^{-1} * (Wt)^{-0.30077})$
SSE	1.084×10^{-5}	(-)

Via optimization, the reaction order (*n*) and reaction rate constant (*K*) was determined simultaneously. Linearization process is then used for calculating the activation energy (*EA*) and the pre-exponential factor (K_o) for the reaction. The Arrhenius-based dependence of the kinetic model is plotted in Figure 6. Plot of *lnK* versus *1/T* gives straight line presented of the oxidation process with a slope equal to *EA/R* and intercept equal to lnK_o. The low value of activation energy obtained in this study indicates that the oxidation of sulphur is faster in the presence of catalyst. The predicted concentration results obtained through modelling within gPROMS program with the experimental results are presented in Table 7.

A comparison between experimental results and model simulated results (applying the generated kinetic parameters obtained via optimization) for oxidation process of light gas oil are plotted in Figures 7(a, b, c, d, e, f) at different process conditions. As can be noticed from these results, the model was found to simulate the performance of trickle bed reactor very well in the range of operation conditions studied among all concentrations with average absolute error less than 5% giving an indication that the mathematical model related to trickle bed reactor for ODS process, can now be applied confidently to reactor design. It has also been noted from these Figures that the conversion increased with increasing in temperature, initial concentration of DBT, and decreasing in LHSV. The increase in conversion happened due to the effect of operating conditions on kinetic parameter used for describing oxidation process . The reaction temperature of the reactor affects the density of LGO, mass velocity of the gases and liquids and viscosity of LGO.

The temperature also influences the rate constant of oxidation processes. Increasing the reaction temperature lead to an increase in reaction rate constant defined by Arrhenius equation and increasing conversion of DBT in the process to sulphone and sluphoxide.

LHSV is also important operational factor that estimates the severity of the reaction and the efficiency of the oxidation process. Decreasing LHSV, the quantity of the reactions rates will be important.

6. Effectiveness Factor

Thiele modulus and Effectiveness factor data obtained from gPROMS program are presented in Table 8. Thiele modulus and effectiveness factor change within very small range. Increasing of DBT concentration increases Thiele modulus values slightly by affecting the values of the rate constant as explained in Figure 8a and 8b. Thus, the increase of DBT concentrations will lead to decrease in the effectiveness factor as shown in Figures 8c and 8d.

The effectiveness factors have been obtained for each process condition. It can be noted that the effectiveness factor is decreased with increasing reaction temperature and *LHSV*. Increasing the temperature (as shown in Figure 8c) means a large increase in the rate constant than the diffusivity leading to a more pronounced diffusion limitation since it becomes the limiting step and hence to smaller effectiveness factors. With increasing *LHSV* at constant temperature, the

decrease in the effectiveness factor can be observed as shown in Figure 8d. This behavior is attributed to the increase in reaction mixture viscosity that is obtained at higher LHSV, since viscosity is directly related with reactants diffusivity and thus with increasing viscosity, the effectiveness factor will be decreased[46].

7. Conclusions

Following observations have been made in this study.

❖ The highest dibenzothiophene conversion (81.2%) was achieved over a homemade catalyst (MnO_2/γ-Al_2O_3) under moderate conditions (Initial concentration = 1000 ppm, temperature = 473 K, and *LHSV*=$1h^{-1}$).

❖ Oxidation reaction of dibenzothiophene in experimental pilot plant trickle-bed reactor loaded with (MnO_2/γ-Al_2O_3) catalyst at different reaction temperatures *LHSV* and initial concentration, has been explained by a rigorous kinetic model to determine the best kinetic parameters. This kinetic model showed that the reaction rate is dominated mainly by temperature and reaction order and that the assumption of first order reaction in previous works is not true.

❖ It was found that dibenzothiophene conversion increased from (32.7% to 81.2%) as LHSV decreased and increasing reaction temperature, leading to enhancement in dibenzothiophene conversion and the catalyst activity.

❖ It was found that the oxidation reaction of dibenzothiophene follows 1.30077 order kinetic with respect to (MnO_2/γ-Al_2O_3) and the activation energy equal to 34.016 kJ/mole.

❖ Oxidative desulphurization process appears to be technically and economically viable for processing ultra-low sulphur fuel from light gas oil feedstock. It can be considered in conjunction with or as substitute for hydrodesulphurization process (HDS). Notably, ODS does not require hydrogen for desulphurization. It is expected that the capital cost and operating cost with ODS would be significantly lower than HDS process (further studies will be investigated in future).

❖ Simulation and optimization help achieving better design and operation of ODS processes. For carrying out meaningful simulation and optimization to create alternative design and operation scenarios cheaply, development of a reliable process model is required by obtaining the best kinetic parameters in trickle bed reactor applied for ODS. For ODS process, an optimization technique, based on minimization of the sum of square errors (*SSE*) between the experimental and model predicted concentrations of sulphur with non-linear (NLN) regression have been used to calculate the best kinetic parameters of these reactions. The kinetic parameters calculated using non-linear regression is found to be more accurate and showed very well agreement with the experimental data with an average absolute error of less than 5% among all results at different operating conditions, which give a clear indication that the models can be

effectively employed to reactor design in addition to predict the concentration profiles of any compound at any conditions.

Nomenclature

$\Delta\rho_p$ Pressure dependence of liquid density, lb/ft^3

$\Delta\rho_T$ Temperature correction of liquid density, lb/ft^3

C_{DBT} Concentration of dibenzothiophene, $cm^3/mole$

C_{in} Initial concentration (inlet to reactor), $cm^3/mole$

C_{out} Final concentration (outlet from reactor), $cm^3/mole$

D_{Ki} Knudsen diffusivity factor, cm^2/sec

D_{ei} Effective diffusivity, cm^2/sec

D_{mi} Molecular diffusivity, cm^2/sec

d_p Particle diameter, cm

d_t Tube diameter, cm

K_o Frequency or pre-exponential factor, $cm^3/g.\ sec$

K_{app} Apparent reaction rate constant, $(time)^{-1}(concentration)^{1-n}$

K_{in} Kinetic rate constant, $(time)^{-1}(\ concentration)^{1-n}$

MW_i Molecular weight of oxygen, g/gmole

Mw_L Molecular weight of liquid phase, g/gmol

r_{DBT} Dibenzothiophene rate of reaction

r_g Mean pore radius, cm

r_p Radius of particle, cm

S_g Specific surface area of particle, cm^2/g

S_P External surface area of catalyst particle, cm^2

$Sp.gr_{15.6}$ Specific gravity of oil at 15.6 ^oC

T_{meABP} Mean average boiling point, R

u_L Velocity of the liquid, cm/sec

V_{CDBT} Critical specific volume of the DBT, ft^3/mole

V_{CL} Critical specific volume of liquid, cm^3/mole

V_{DBT} Molar volume of DBT at n.b. temperature, cm^3/mole

V_g Total pore volume, cm^3/g

V_L Molar volume of liquid at its n.b. temperature, cm^3/mole

V_P Volume of catalyst particle, cm^3

μ_L Dynamic viscosity of liquid phase, mPa. sec

$\rho_{15.6}$ Density of light gas oil at 15.6 ^oC, g/cm^3

ρ_B Bulk density, g/cm^3

ρ_L Liquid density at process condition, lb/ft^3

ρ_o Density of light gas oil at 15.6 ^oC and 101.3 Kpa, lb/ft^3

ρ_p Particle density, g/cm^3

a Dimensionless number

EA Activation energy, kJ/mole

F_{DBT} Input of dibenzothiophene, moles/time

g Acceleration, cm/sec^2

K Reaction rate constant, $h^{-1}*wt^{(n-1)}$

n Order of reaction kinetic

ppm Part per million

R Universal gas constant, 8.314 J/mol. K

T Temperature, K or ^oC

V Bed volume of particle catalyst, cm^3

V_L Volumetric flow of liquid phase, cm^3/time

V_P Pore volume, cm^3

τ Residence time, h

Greek letters

η_{ce} External catalyst wetting efficiency

ϵ_S Catalyst porosity

$\mathcal{T}$ Tortuosity factor

Φ Thiele modulus

ϵ_B Bed void fraction

References

(1) Hasan, Z.; Jeon, J.; Jhung, SH. *J. Hazard Mater* **2012**, 205–206, 216–21.

(2) Ma, X.; Sakanishi, K.; Mochida, I. *Ind. Eng. Chem. Res*. **1994**, 33, 218–222.

(3) Song, C.; Ma, X. *Appl. Catal. B* **2003**, 41, 207-238.

(4) Jiang, C.Y.; Wang, J.J.; Wang, S.T.; Guan, H.Y.; Wang, X.H.; Huo, M.X. *Appl. Catal. B* **2011**, 106, 343-349.

(5) Zhang, B.Y.; Jiang, Z.X.; Li, J.; Zhang, Y.N.; Lin, F.; Liu, Y.; Li C. *J. Catal.* **2012**, 287, 5-12.

(6) Verdia, P.; Gonzalez, E.J.; Rodriguez-Cabo, B.; Tojo, E. *Green Chem*. **2011**, 13, 2768-2776.

(7) Rodriguez-Cabo, B.; Francisco, M.; Soto, A.; Arce, A. *Fluid Phase Equilib*. **2012**, 314, 107-112.

(8) Aida, T.; Yamamoto, D. *Prepr. Pap. Am. Chem. Div. Fuel Chem.* **1994**, 39, 623-629.

(9) Wang, D.; Qian, E.W.; Amano, H.; Okata, K.; Ishihara, A.; Kabe, T. *Appl. Catal. A Gen.* **2003**, 253, 91–99.

(10) Murata, S.; Murata, K.; Kidena, K.; Nomura, M.A. *Energy Fuels* **2004**, 18, pp. 116–121.

(11) Trakarnpruk, W.; Rujiraworawut, K. *Fuel Process. Technol.* **2009**, 90, 411–414.

(12) Jin, C.Z.; Li, G.; Wang, X.Sh.; Zhao, L.X.; Liu, L.P.; Liu, H.O.; Liu, Y.; Zhang, W.P.; Han, X.W.; Bao, X.H. *Chem. Mater.* **2007**, 19, 1664–1670.

(13) Wang, D.; Qian, E.W.; Amano, H.; Okata,K.; Ishihara, A.; Kabe, T. *Appl. Catal. A* **2003**, 253, 91–99.

(14) Lu, H.Y.; Gao, J.B.; Jiang, Z.X.; Yang, Y.X.; Song, B.; Li, C. *J. Catal.* **2006**, 239, 369–375.

(15) Qiu, J.H.; Wang, G.H.; Zeng, D.L.; Tang, Y.; Wang, M.; Li, Y.J. *Fuel Process. Technol.* **2009**, 90, 1538–1542.

(16) Giuseppe, A.D.; Crucianelli, M.; Angelis, F.D.; Crestini, C.; Saladino, R. *Appl. Catal. B* **2009**, 89, 239–245.

(17) Ishihara, A.; Wang, D.H.; Dumeignil, F.; Amano, H.; Qian, E.W.; Kabe, T. *Appl. Catal. A* **2005**, 279, 279–287.

(18) Sampanthar, J.T.; Xiao, H.; Dou, J.; Nah, T.Y.; Rong, X.; Kwan**,** W.P. *Applied Catalysis B: Environmental* **2006**,, 63, pp. 85–93.

(19) Sundararaman, R.; Song, C. *Industrial & Engineering Chemistry Research* **2014**, 53, 1890-1899.

(20) Alcaraz, J.J.; Arena, B.J.; Gillespie, R.D.; Holmgren, J.S. *Catalysis Today* **1998**, 43, 89-99.

(21) Wang, B.; Zhu, J.; Ma, H. *Journal of Hazardous Materials* **2009**, 164, 256–264.

(22) Gonzalez - Garcia, O.; Cedeno - Caero, L. *Catalysis Today* **2009**, 148, 42–48.

(23) Zannikos, F.; Lois, E.; Stournas, S. *Fuel processing technology* **1995**, 42, 35 – 45.

(24) Ramırez-Verduzco, L.F.; Torres-Garcıa, E.; Gomez-Quintana, R.; Gonzalez- Pena, V.; Murrieta-Guevara, F. *Catalysis Today* **2004**, 98, 289–294.

(25) Yang, L.; Li, J.; Yuan, X.; Shen, J.; Qi, Y. *Journal of Molecular Catalysis A: Chemical* **2007**, 262, 114–118.

(26) Nanoti, A.; Dasgupta, S.; Goswami, A.N.; Nautiyal, B.R.; Rao, T.V.; Sain, B.; Sharma, Y.K.; Nanoti, S.M.; Garg, M.O.; Gupta, P. *Micro-porous and Mesoporous Materials* **2009**, 124, 94–99.

(27) Etemadi, O.; Yen, T.F. *Energy Fuels* **2007**, 21, 1622-1627.

(28) Nigam, K.D.P.; Larachi, F. *Chem. Eng. Sci.* **2005**, 60, 5880-5894.

(29) Bej, S.K.; Dalai, A.; K.; Adjaye, J. *Energy Fuels* **2001**, 15, 377-383.

(30) Wärnå, J.; Salmi, T. *Comput. Chem. Eng.* **1996**, 20, 39 – 47 .

(31) Al-Dahhan, M.H. *Proceedings–International Symposium on Advances in Hydro processing of Oil Fractions*. Morelia, Mexico, June 2007; pp. 26-29.

(32) Dudukovic, M.P. *AIChE J.* **1977**, 23, 940–944.

(33) Froment, G.F.; Bischoff, K.B. Chemical Reactor Analysis and Design; John Wiley and Sons Inc.: New York, 1990.

(34) Macı´as, M.J.; Ancheyta, J. *Catal. Today* **2004**, 98, 243-252.

(35) Mederos, F.S.; Elizaldi, G.; Ancheyta, J. *Catalysis Review* **2009**, 51, 485-607.

(36) Mederos, F.S.; Rodrı´guez, M.A.; Ancheyta, J.; Arce, E. *Energy Fuels* **2006**, 20, 936-945.

(37) Jarullah, A.T.; Mujtaba, I.M.; Wood, A.S. *Chem. Eng. Sci*. **2010**, 66, 859–871.

(38) Ahmed, T. Hydrocarbon Phase Behavior; Gulf Publishing: Houston, 1989.

(39) Al-Dahhan, M.H.; Dudukovic, M.P. *Chem. Eng. Sci.* **1995**, 50, 2377-2389.

(40) Froment, G.F.; Bischoff, K.B. *Chemical Reactor Analysis and Design*; Wiley: New York, 1990..

(41) Jarullah, A.T.; Mujtaba, I.M.; Wood, A.S. *Applied Energy* **2012**, 94, 182–191.

(42) Jarullah, A.T.; Mujtaba, I.M.; Wood, A.S. *Fuel* **2011**, 90, 2165–2181.

(43) Jimenez, F.; Nunez, M.; Kafarov, V. *Chemical Engineering Journal* **2007**, 134, 200-208.

(44) Buzzi-Ferraris, G.; Manenti, F. *Chemical Engineering* Science *2009*, 64, 1061-1074

(45) Buzzi-Ferraris, G.; Manenti, F. *Computers & Chemical Engineering 2010*, 34, 1904-1906

(46) Martnez, J.; Ancheyta, J. *Fuel* **2012**, 100, 193-199.

List of Tables

List of Figures

Table 1: Specification analysis of light gas oil.

Physical property	Light gas oil
Specific gravity	0.851
Viscosity (sct) at (293K)	4.9
Flash point,(^{o}C)	55
Total sulphur, (ppm)	9.8
Cetane index	52
Colour	0.5
Pour point,(^{o}C)	-39
API gravity	34.8

Table 2: Properties of active compounds.

Chemicals and Materials	Purity%	Function	Manufacture
Manganese acetate $Mn(CH_3COO)_2.4H_2O$	>98	Active material	Sigma
deionized water	-	Solvent of Active material	Samarra company

Table 3: Experimental device description and properties.

Description	**Specification**
Feed tank (diesel)	Box, 10 litter
Compressor	15 bar
Pump	Dosapor Milton Roy/Italy Max. flow=1.27 litter/hour Max. Pressure=20 bar
Preaheter	Electrical coil
Trickle bed reactor	Stainless steel (SS) 310 1.6 cm * 73 cm
Control box	Control box
Reactor heating jacket	Electrical coil
Heat exchanger	Shell and tube (Four tubes) stainless steel
Separator	Stainless steel
Pressure gauge	Nue-tec/Italy (0-25bar)
Gas flow meter	Yamamoto (0-6 litter/min)
Cooling water	20 ^{o}C

Table 4: Values of constant parameters and specified variables used in the model.

Parameter	Symbol	Unit	Value
Initial concentration	CA, CB, CC	wt	CA=0.1, CB= 0.08, CC= 0.05
Temperature	T1, T2, T3,	K	T1= 403, T2= 443, T3= 473
Liquid hour space velocity	LHSV1, LHSV2, LHSV3	h^{-1}	LHSV1=1, LHSV2=2, LHSV3=3
Pressure	P	Psia	14.7
Density of LGO at 15.6 ^{o}C and 101.3 kPa	Den0	Ib/ft^3	52.58307119
Gas constant	R	J/mole. K	8.314
Volume of catalyst particle	V_p	cm^3	0.00214
Total geometric external area of particle	S_p	cm^2	0.0804
Bulk density	$\rho_{B\,Mn}$	g/cm^3	$\rho_{B\,Mn} = 0.7188$
pore volume per unit mass of catalyst	V_g	cm^3/g	$V_{g\,Mn} = 0.476$
Molecular weight of oxygen	MW_i	g/gmole	0.21
Molecular weight of LGO	MW_L	g/gmole	212.12
Critical specific volume of the DBT compound	V_{CDBT}	ft^3/mole	8.2176
Mean average boiling point	T_{meABP}	R	981.27
Specific surface area of particle	S_g	cm^2/g	S_{gMn}= 2120000
Tube diameter	d_t	cm	1.6
Velocity of LGO	u_{L1}, u_{L2}, u_{L3}	cm/sec	u_{L1}=0.00799, u_{L2}= 0.01599, u_{L3}= 0.02368
Acceleration gravity	g	cm/sec^2	981

Table 5: Experimental results obtained at different operation conditions (T, LHSV and I.C).

I.C (ppm)	Temperature (K)	LHSV (h^{-1})	DBT concentration (ppm)	DBT conversion
1000	403	1	672.65	0.32
1000	403	2	748.32	0.25
1000	403	3	850.62	0.14
1000	443	1	465.76	0.53
1000	443	2	624.36	0.37
1000	443	3	715.29	0.28
1000	473	1	188.12	0.81
1000	473	2	390.82	0.60
1000	473	3	488.75	0.51
800	403	1	560.26	0.29
800	403	2	620.62	0.22
800	403	3	706.35	0.11
800	443	1	392.98	0.50
800	443	2	512.30	0.36
800	443	3	629.26	0.21
800	473	1	175.27	0.78
800	473	2	329.98	0.58
800	473	3	435.46	0.45
500	403	1	359.67	0.28
500	403	2	392.76	0.21
500	403	3	448.65	0.10
500	443	1	260.26	0.47
500	443	2	339.86	0.32
500	443	3	408.68	0.18
500	473	1	132.53	0.73
500	473	2	217.47	0.56
500	473	3	271.98	0.45

Table 6: Comparison between experimental product and predicted product.

LHSV(h^{-1})	I.C(ppm)	Temperature (K)	Predicted	Experimental	Error%
1	1000	403	862.75	672.65	28.26
1	1000	443	760.06	465.76	63.18
1	1000	473	569.82	188.12	202.89
1	800	403	706.65	560.26	26.12
1	800	443	634.00	392.98	61.33
1	800	473	492.78	175.27	181.14
1	500	403	459.06	359.67	27.63
1	500	443	425.01	260.26	63.29
1	500	473	352.65	132.53	166.09
2	1000	403	919.54	748.32	22.88
2	1000	443	852.74	624.36	36.57
2	1000	473	710.33	390.82	81.75
2	800	403	745.76	620.62	20.16
2	800	443	699.67	512.30	36.57
2	800	473	597.93	329.98	81.19
2	500	403	476.56	392.76	21.33
2	500	443	455.79	339.86	34.10
2	500	473	407.21	217.47	87.25
3	1000	403	941.94	850.62	10.73
3	1000	443	891.76	715.29	24.67
3	1000	473	778.14	488.75	59.20
3	800	403	763.08	706.35	8.03
3	800	443	730.46	629.26	16.08
3	800	473	654.00	435.46	50.18
3	500	403	483.24	448.65	7.71
3	500	443	468.03	408.68	14.52
3	500	473	414.43	271.98	52.37

Table 7: Simulation and experimental results.

LHSV(h^{-1})	I.C(ppm)	Temperature (K)	Concentration by Simulation	Conversion by Simulation	Experimental Concentration	Experimental Conversion	Error%
1	1000	403	655.54	0.34	672.65	0.32	2.60
1	1000	443	483.87	0.51	465.76	0.53	3.74
1	1000	473	197.66	0.80	188.12	0.81	4.82
1	800	403	538.03	0.32	560.26	0.29	4.13
1	800	443	403.68	0.49	392.98	0.50	2.65
1	800	473	171.78	0.78	175.27	0.78	2.03
1	500	403	353.24	0.29	359.67	0.28	1.81
1	500	443	273.68	0.45	260.26	0.47	4.90
1	500	473	126.44	0.74	132.53	0.73	4.81
2	1000	403	786.57	0.21	748.32	0.25	4.86
2	1000	443	656.88	0.34	624.36	0.37	4.94
2	1000	473	372.83	0.62	390.82	0.60	4.82
2	800	403	638.70	0.20	620.62	0.22	2.83
2	800	443	538.94	0.32	512.30	0.36	4.94
2	800	473	314.95	0.60	329.98	0.58	4.77
2	500	403	410.73	0.17	392.76	0.21	4.37
2	500	443	353.63	0.29	339.86	0.32	3.89
2	500	473	218.92	0.56	217.47	0.56	0.66
3	1000	403	842.63	0.15	850.62	0.14	0.94
3	1000	443	739.43	0.26	715.29	0.28	3.26
3	1000	473	484.95	0.51	488.75	0.51	0.78
3	800	403	687.36	0.14	706.35	0.11	2.76
3	800	443	611.76	0.23	629.26	0.21	2.86
3	800	473	418.58	0.47	435.46	0.45	4.03
3	500	403	434.68	0.13	448.65	0.10	3.21
3	500	443	390.15	0.22	408.68	0.18	4.75
3	500	473	273.74	0.45	271.98	0.45	0.64

Table 8: Effectiveness factor results (at I.C of 1000, 800, 500 ppm with different T and LHSV).

Concentration(ppm)	*LHSV* (h^{-1})	Temperature (K)	Effectiveness factor η (%)
1000	1	403	98.85
1000	1	443	97.97
1000	1	473	96.94
1000	2	403	98.79
1000	2	443	97.78
1000	2	473	96.33
1000	3	403	98.77
1000	3	443	97.71
1000	3	473	96.04
800	1	403	98.92
800	1	443	98.08
800	1	473	97.06
800	2	403	98.86
800	2	443	97.91
800	2	473	96.49
800	3	403	98.84
800	3	443	97.83
800	3	473	96.20
500	1	403	99.05
500	1	443	98.28
500	1	473	97.31
500	2	403	99.00
500	2	443	98.15
500	2	473	96.85
500	3	403	98.99
500	3	443	98.09
500	3	473	96.64

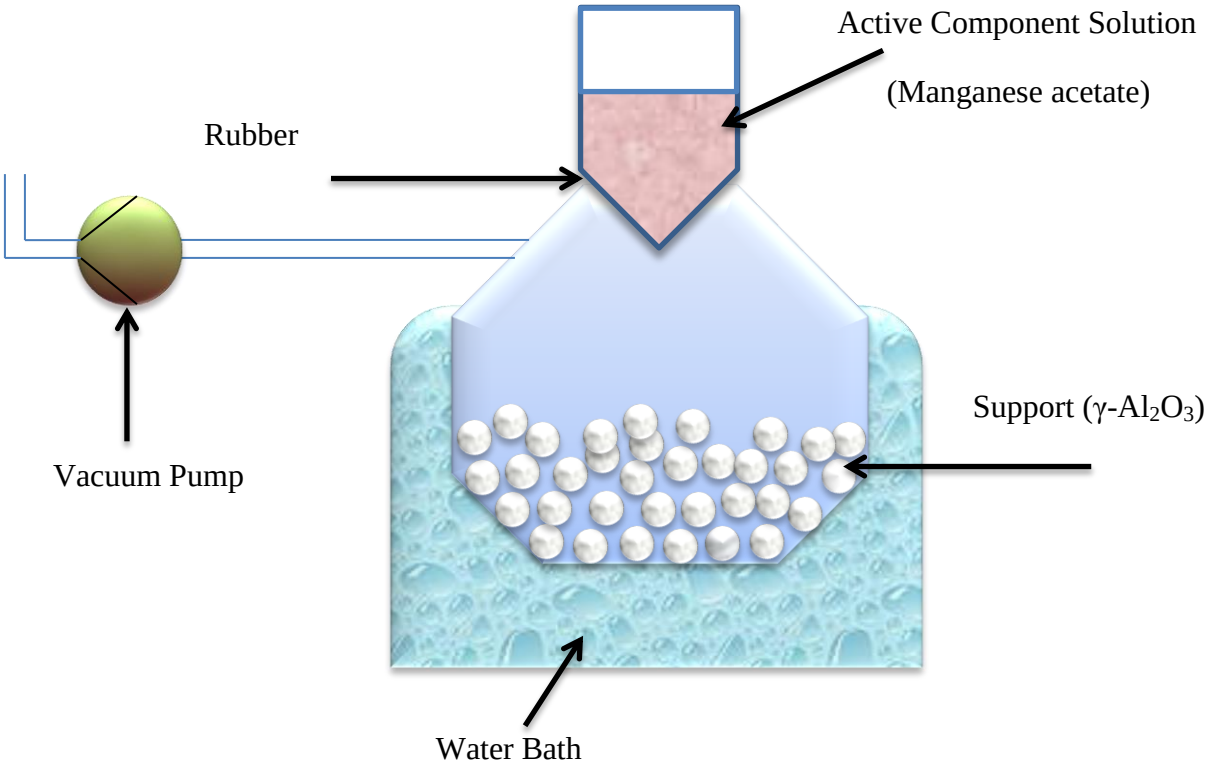
Active Component Solution
(Manganese acetate)
Rubber
Support (γ-Al2O3)
Vacuum Pump
Water Bath

Figure 1

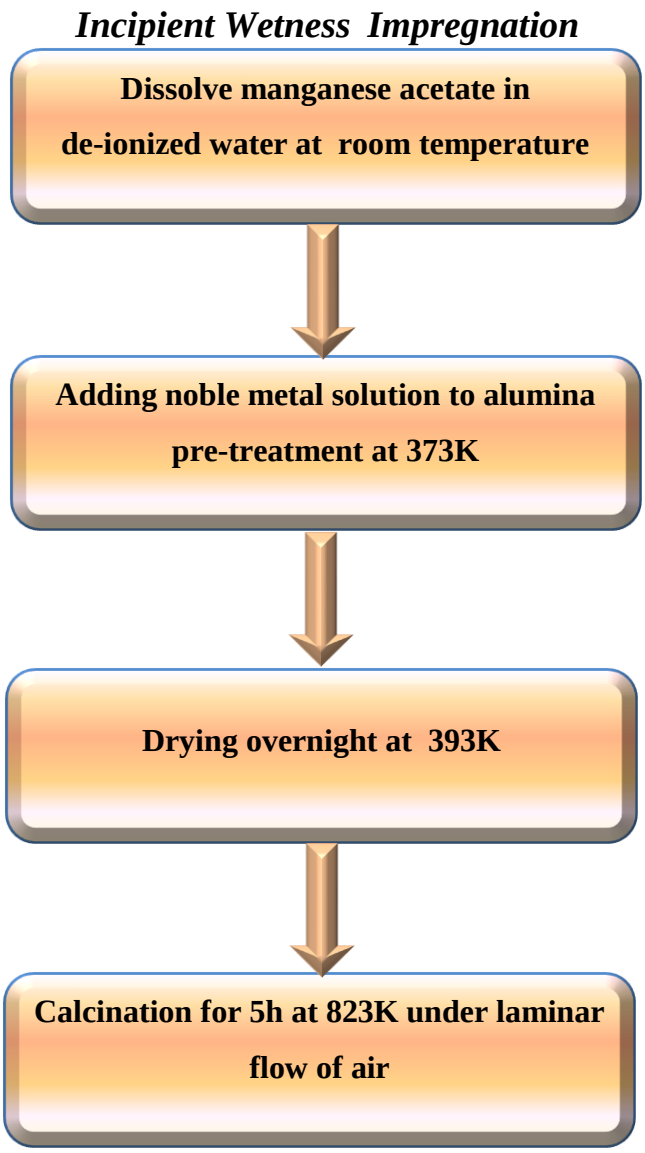
Incipient Wetness Impregnation
Dissolve manganese acetate in de-ionized water at room temperature
Adding noble metal solution to alumina pre-treatment at 373K
Drying overnight at 393K
Calcination for 5h at 823K under laminar flow of air

Figure 2

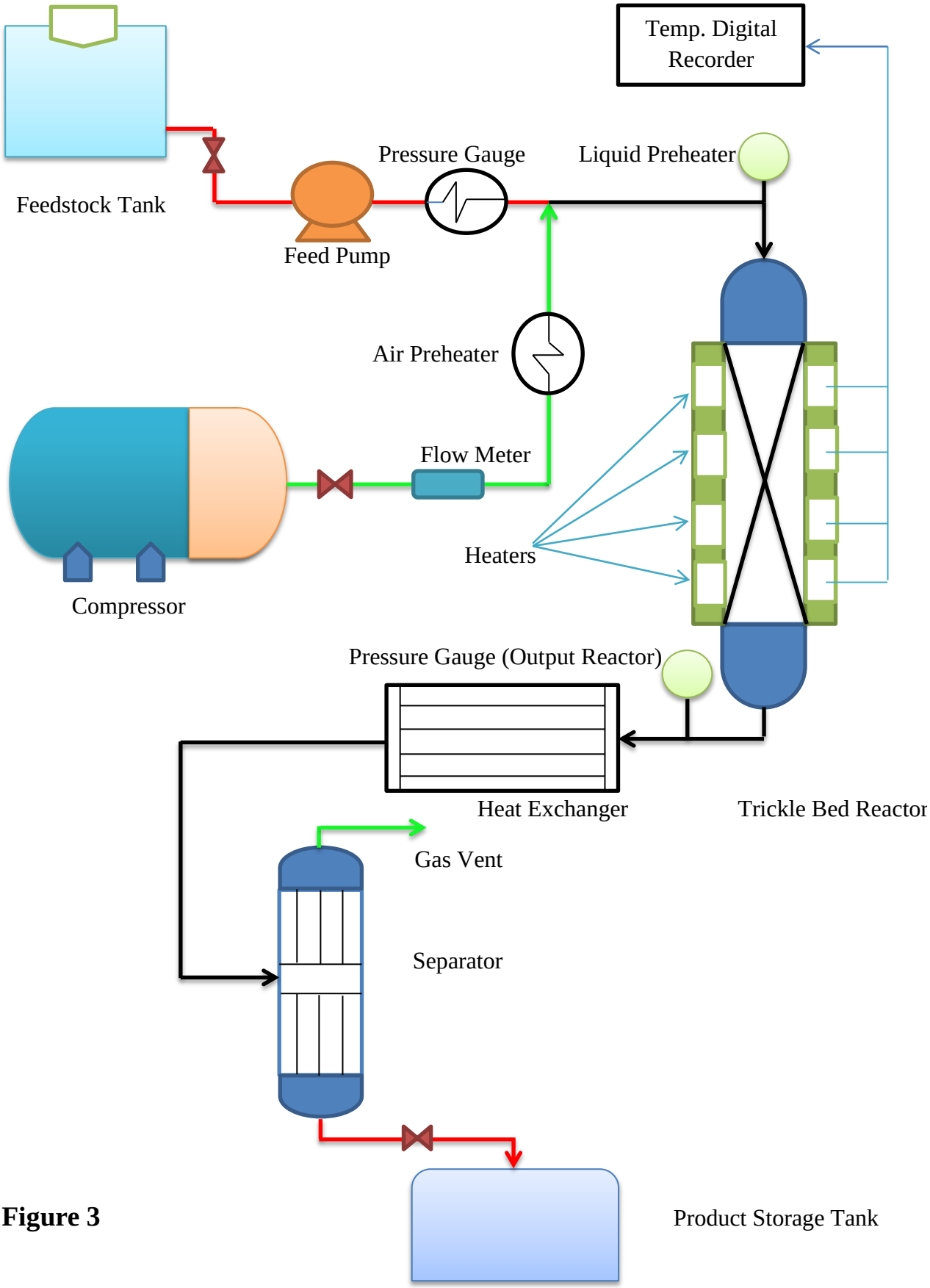
Temp. Digital Recorder
Pressure Gauge
Liquid Preheater
Feedstock Tank
Feed Pump
Air Preheater
Flow Meter
Heaters
Compressor
Pressure Gauge (Output Reactor)
Heat Exchanger
Trickle Bed Reactor
Gas Vent
Separator
Product Storage Tank

Figure 3

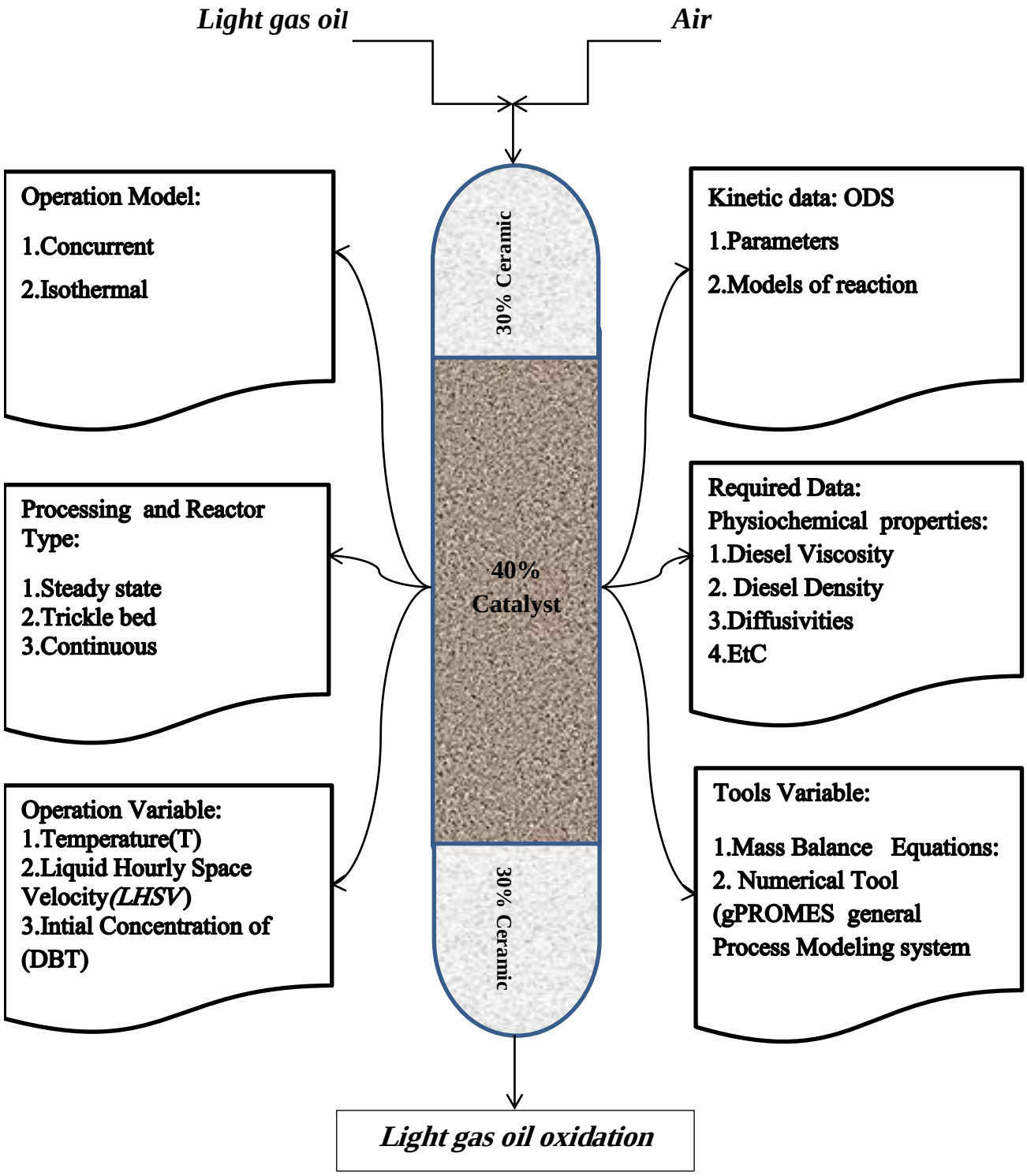
Light gas oil
Air
Operation Model:
1.Concurrent
2.Isothermal
Kinetic data: ODS
1.Parameters
2.Models of reaction
30% Ceramic
Processing and Reactor Type:
1.Steady state
2.Trickle bed
3.Continuous
40% Catalyst
Required Data:
Physiochemical properties:
1.Diesel Viscosity
2. Diesel Density
3.Diffusivities
4.EtC
Operation Variable:
1.Temperature(T)
2.Liquid Hourly Space Velocity(LHSV)
3.Intial Concentration of (DBT)
30% Ceramic
Tools Variable:
1.Mass Balance Equations:
2. Numerical Tool (gPROMES general Process Modeling system
Light gas oil oxidation

Figure 4

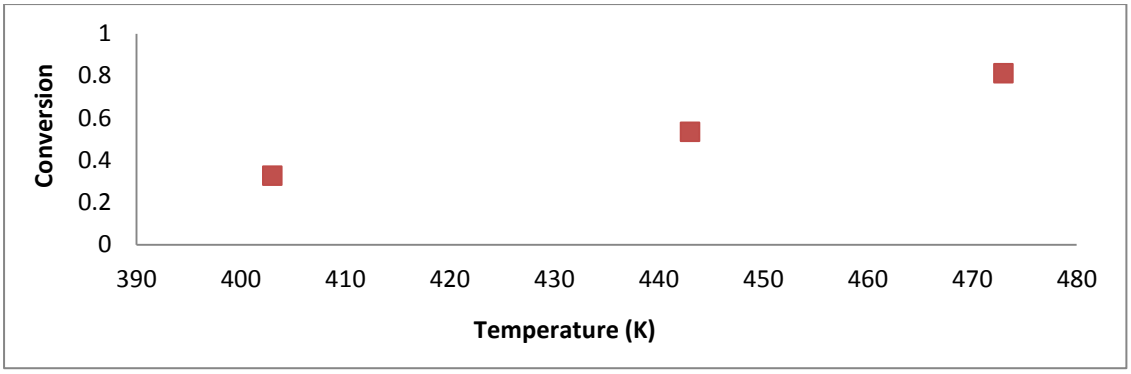

(a)

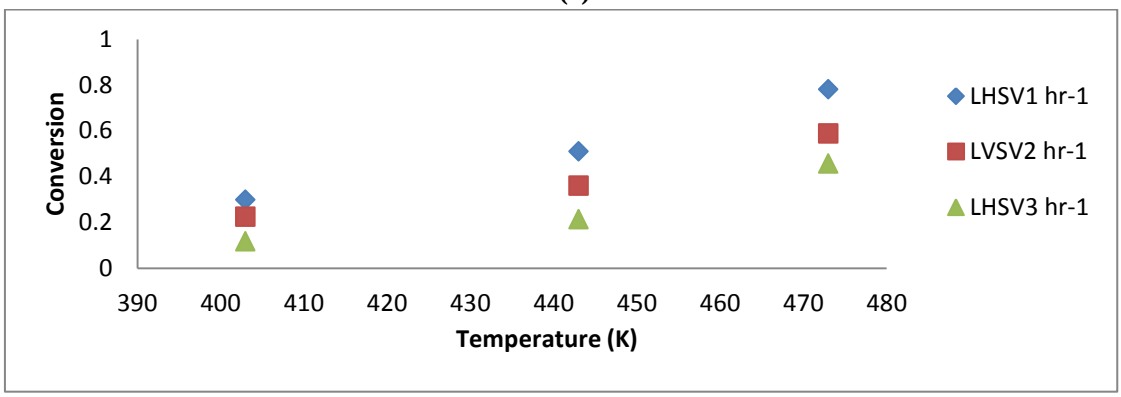

(b)

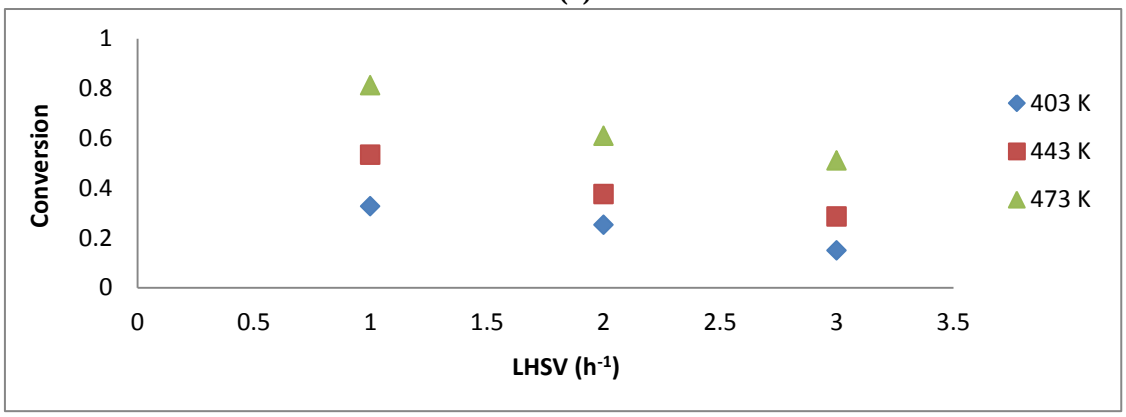

(c)

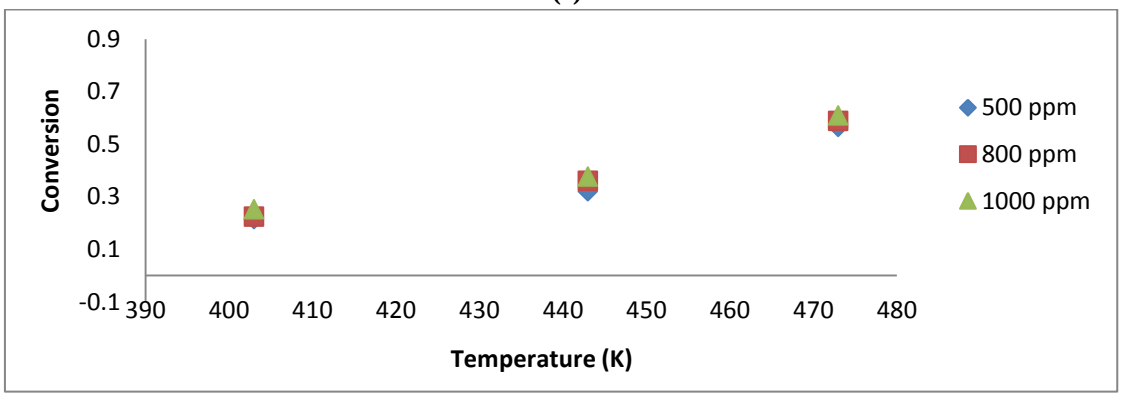

(d)

Figure 5

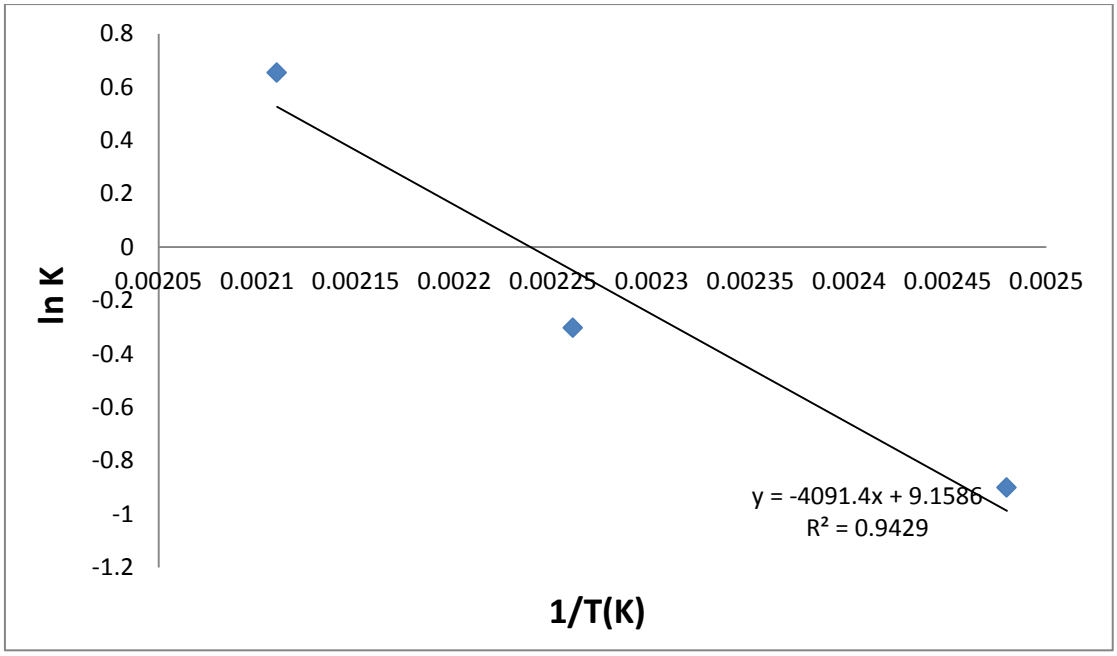
0.8
0.6
0.4
0.2
0
-0.2
-0.4
-0.6
-0.8
-1
-1.2
ln K
0.00205
0.0021
0.00215
0.0022
0.00225
0.0023
0.00235
0.0024
0.00245
0.0025
1/T(K)
y = -4091.4x + 9.1586
R² = 0.9429

Figure 6

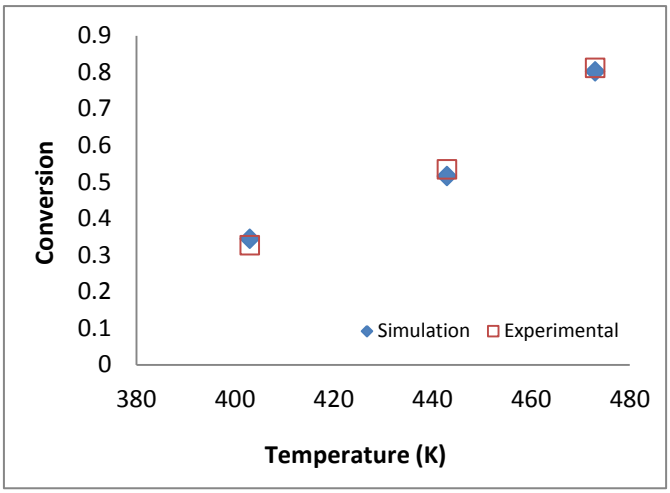

(a)

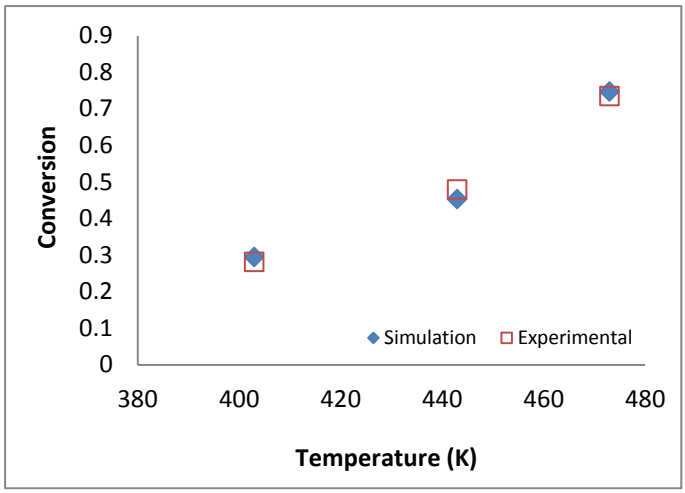

(b)

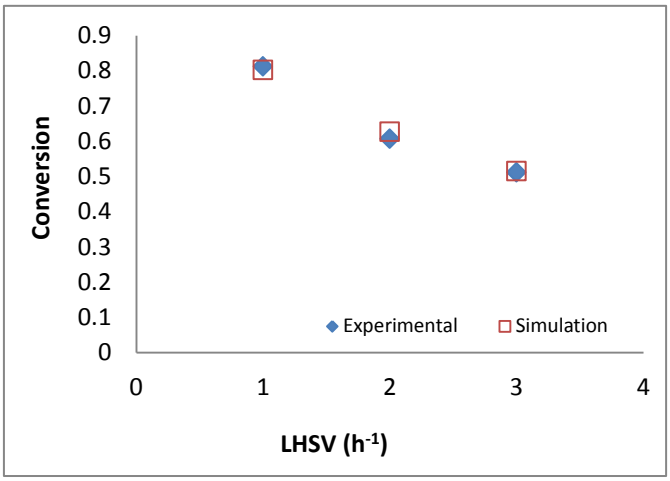

(c)

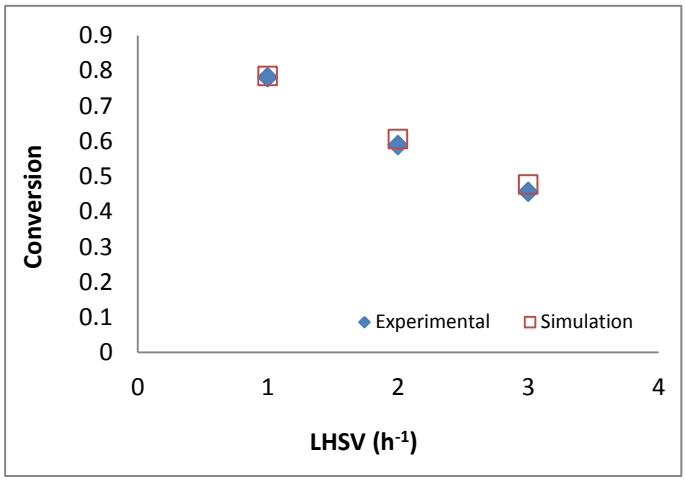

(d)

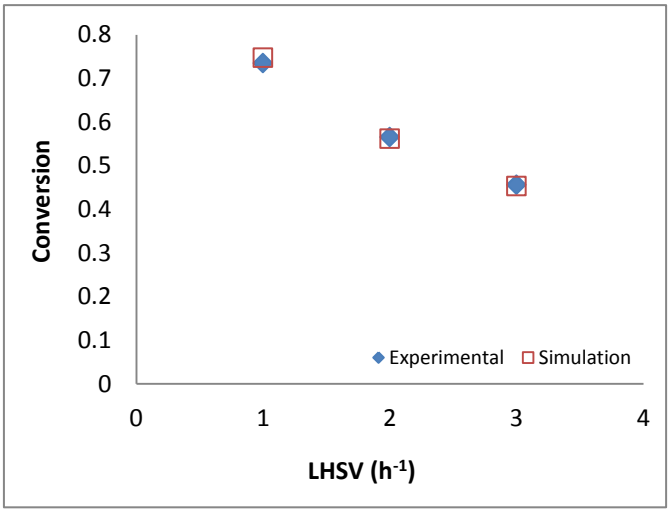

(e)

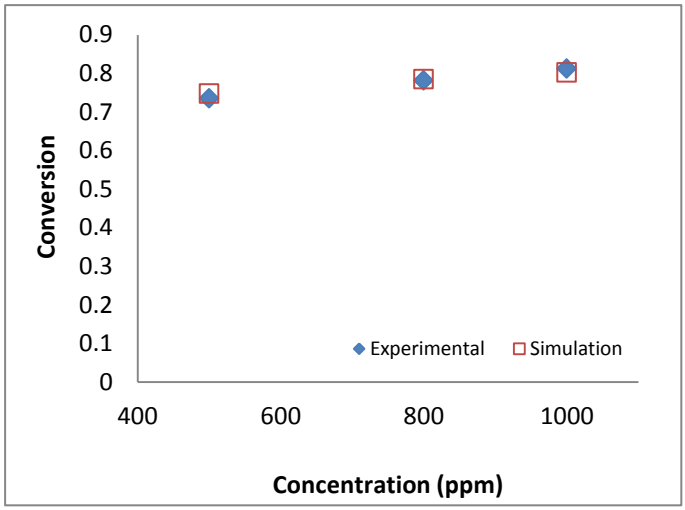

(f)

Figure 7

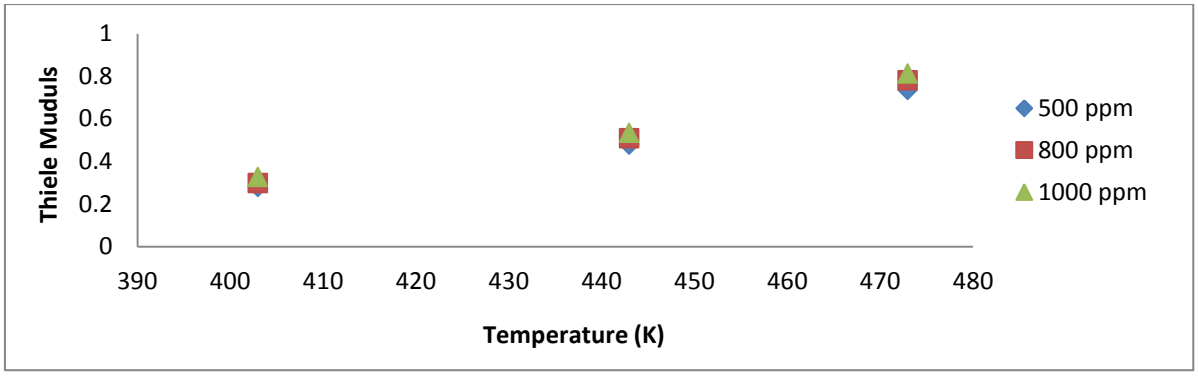

(a)

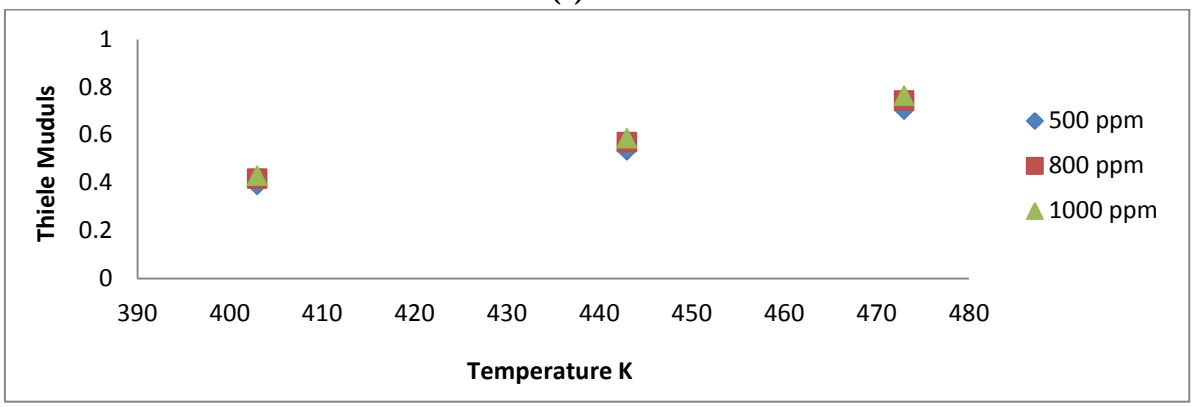

(b)

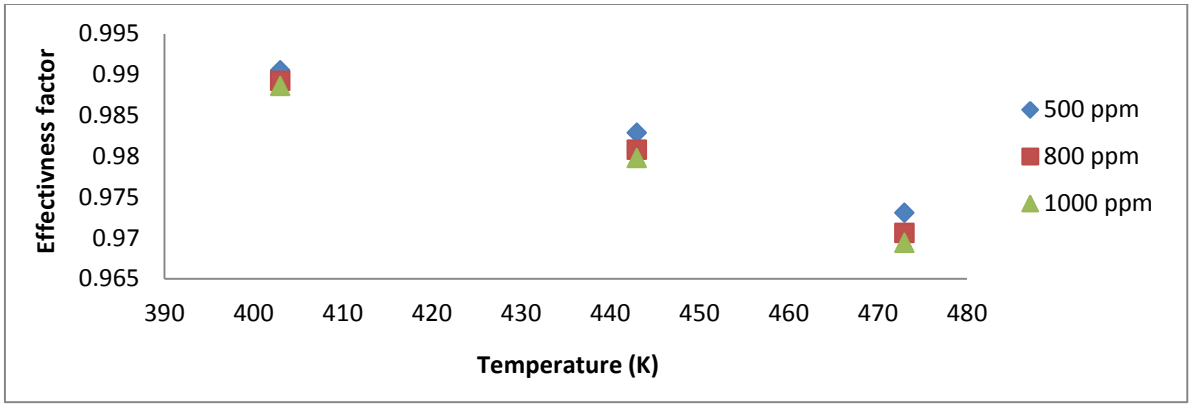

(c)

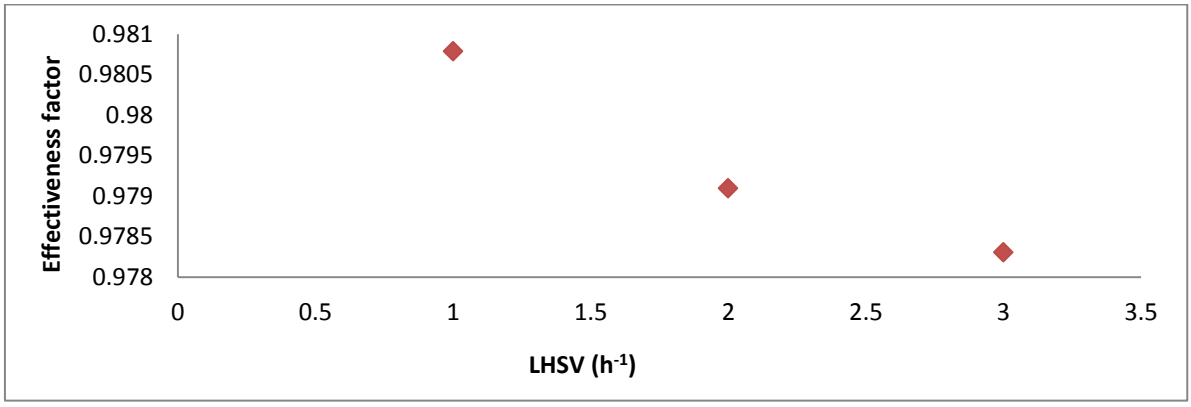

(d)

Figure 8